Coastline Detection Based on Sentinel-1 Time Series for Ship- and Flood-Monitoring Applications

Ramona Pelich, *Member, IEEE*, Marco Chini, *Senior Member, IEEE*, Renaud Hostache, Patrick Matgen, and Carlos López-Martínez, *Senior Member, IEEE*

***Abstract*— This letter addresses the use of the Sentinel-1 time series with the aim of proposing an automatic and unsupervised coastline detection method that averages the dynamical variations of coastal areas over a limited period of time, e.g., one year. First, we propose applying a temporal averaging filter that allows the temporal variations in coastal areas, e.g., due to tides or vegetation, to be encapsulated, and, at the same time, the speckle to be reduced, without decreasing the spatial resolution of the synthetic aperture radar (SAR) time series. Then, based on the distinctive backscattering values of the sea and land pixels, we will employ an iterative hierarchical tiling method in order to accurately characterize the two classes using bimodal distribution. The distribution is then segmented by a thresholding and region-growing procedure to separate the sea and land classes. A large-scale quantitative comparison between the SAR-derived and open street map (OSM) coastlines allows for a numerical evaluation of the results, i.e., an overall agreement ranging from 80% to 90%. In addition, Sentinel-2 images are used to evaluate the estimated SAR coastline qualitatively. Furthermore, the benefits of having an accurate SAR coastline are shown in the case of two well-known Earth observation-monitoring applications, ship detection, and floodwater mapping.**

***Index Terms*— Bimodal distribution, coastline, multitemporal, region growing, synthetic aperture radar (SAR).**

I. Introduction

COASTAL areas represent very diverse and dynamic zones across the globe. As stated by the United Nations (UN) Atlas of the Oceans [1], nowadays, approximately 44% of the world's population lives within 150 km of the coast. Coastal zones are used for human settlement, agriculture, trade, industry, and amenities [2], therefore playing an important role in the global economy. For this reason, it is important to have access to accurate information about these areas. For instance, the detection and monitoring of the coastline are of great importance for both maritime surveillance activities and studying coastal environment spatiotemporal changes, e.g., erosion and sedimentation. Earth observation (EO) has been used to detect coastlines in a variety of scientific techniques applied operationally, providing information about their geographical extent and characteristics at a global level [3]. This information is essential for tackling the challenges of environmental monitoring applications, including ship detection in the coastline proximity [4] and coastal flood mapping [5].

Synthetic aperture radar (SAR) sensors occupy a privileged place among EO sensors due to their quasi all-weather and day/night observation capabilities. Numerous studies propose algorithms enabling the detection/extraction of coastlines from SAR observations. A pioneering study in the SAR research field [6] proposes coupling basic image-processing techniques with edge tracing algorithms in order to solve the coastline detection challenge from Seasat and SIR-B SAR images. A semiautomatic method of shoreline delineation from ERS-1 SAR images was proposed in [7]. First, the sea regions are detected based on their low edge density at coarse resolution, and then, the areas near the shoreline are processed at high resolution by using an active contour model. Other research studies propose using wavelet methods [8] or region-based set levels coupled with the expectation–maximization algorithm [9] to estimate the probability density functions (PDFs) of the land and water classes to be separated. Another unsupervised method, based on the Bayesian stochastic estimation and the Markov random field (MRF) frameworks applied to image stacks, is proposed in [10]. Alternatively, polarimetry-based approaches are also able to efficiently delineate the coastline from SAR imagery. A first polarimetry-based study proposes applying the constant false alarm rate (CFAR) thresholding and a Sobel edge detector to a set of multipolarization COSMO-SkyMed images in order to investigate the land/sea discrimination for different polarization configurations [11]. The use of the correlation between the copolarized HH and VV channels, followed by two Gaussian-shaped filters in the polarimetric domain, allows the coastline to be extracted from COSMO-SkyMed SAR images, as demonstrated in [12]. Later, a related study, aiming to assess the extraction of the waterlines from single- and dual-polarimetric data and based on multiscale normalized cut segmentation and the VV/HH correlation, respectively, is proposed in [13]. More recent studies demonstrate that region-edge-based active contour models combined with ratio edge detectors [14] or local spectral histogram and level set techniques [15] also enable accurate detection of shorelines by using Radarsat-2 and TerraSAR-X images. In addition to the abovementioned research studies, new SAR-based coastline mapping techniques have emerged from the recent advances in SAR imaging capabilities, such as those of the Sentinel-1 SAR mission. For instance, a fuzzy clustering method based on the mean and standard deviation parameters [16] or a modified K-means method coupled with an adaptive object-based region-merging mechanism [17]

Manuscript received December 15, 2019; revised May 29, 2020; accepted June 29, 2020. Date of publication July 20, 2020; date of current version September 27, 2021. This work was supported in part by the Luxembourg National Research Fund (FNR) through Vessel monitoring and kinematic modelling based on satellite Earth Observation and ground measurements (SKUA) under Grant 11610378 and in part by MOnitoring and predicting urban flood using Sar InTerferometric Observations (MOSQUITO) under Project C15/SR/10380137. *(Corresponding author: Ramona Pelich.)*

Ramona Pelich, Marco Chini, Renaud Hostache, and Patrick Matgen are with the Department of Environmental Research and Innovation (ERIN), Luxembourg Institute of Science and Technology (LIST), 4422 Belvaux, Luxembourg (e-mail: ramona.pelich@list.lu; marco.chini@list.lu; renaud.hostache@list.lu; patrick.matgen@list.lu).

Carlos López-Martínez is with the Department of Signal Theory and Communications (TSC), Universitat Politecnica de Catalunya (UPC), 08034 Barcelona, Spain (e-mail: carlos.lopez@tsc.upc.edu).

Color versions of one or more of the figures in this letter are available online at https://ieeexplore.ieee.org.

Digital Object Identifier 10.1109/LGRS.2020.3008011

are applied to Sentinel-1 imagery to extract the coastline. The Sentinel-1 dual-polarization characteristics are also employed in unsupervised methods, based on the correlation between copolarized and cross-polarized channels, to delineate the shorelines [18], [19]. The derived coastline can be used to assess temporal changes by applying the proposed methods [19], [20] to individual images from Sentinel-1 time series. The accuracy achieved by state-of-the-art algorithms is generally estimated through comparisons with manually traced coastlines or ancillary information, including global positioning system data. For example, in [17], 93% of the Sentinel-1 coastline lies within a 2-pixel distance in comparison with the manually traced one.

In the abovementioned state-of-the-art studies, single SAR acquisitions are employed to extract the coastline. Therefore, the SAR-estimated coastline characterizes a coastal area as it appears at the time the SAR image was acquired, without considering any dynamical effects of such areas, e.g., tides. In addition, SAR-based coastline detection remains challenging due to the presence of speckle noise, the complexity of coastal land covers, and sea state variations [11], [21]. Therefore, we propose employing multitemporal SAR filtering to take into account constantly occurring coastal dynamical effects and, at the same time, reduce the speckle. Moreover, in order to extract the coastline in an accurate and efficient manner [22], we propose an adaptive hierarchical-based automatic classification procedure, i.e., hierarchical split based tiling approach (HSBA), that allows us to efficiently separate the sea and land classes under dynamic temporal scenarios [23].

II. Methodology

In this study, we define the coastline as a geographical variable/map with constant dynamical variations within a limited period of time, e.g., one year. The dynamical variations include periodical coastal changes, due for example to tides, waves, or currents that occur systematically (e.g., daily) or permanent changes generated by vegetated coastal areas (e.g., deltas and wetlands), erosion/sedimentation processes, or human interventions (e.g., dikes and walls) with evolution over a longer time scale, ranging from weeks to months. The coastline is defined as a geographical variable that encompasses the average of all periodical changes and the most significant permanent changes by making use of the SAR image time series acquired over one year. We suppose that in a time series spanning one year, the most relevant and representative dynamics influencing the location of the coastline will be considered. In this framework, the Sentinel-1 mission is particularly well suited to computing the coastline from the SAR time series due to its short repeat pass (six days). This Sentinel-1 characteristic allows image stacks to be generated for nearly all the coastal regions across the globe with a regular frequency of every few months, depending on the Sentinel-1 acquisition plan. Based on the Sentinel-1 stacks, we propose a coastline detection technique composed of three main steps: 1) multitemporal filtering; 2) image tiling for bimodal tile selection; and 3) estimation of the bimodal distribution parameters and image segmentation. Each step is described in the following paragraphs, while the entire procedure of the Sentinel-1 based coastline detector is summarized in the flowchart given in Fig. 1.

It is well known that SAR images are affected by speckle noise, which deteriorates their radiometric resolution. Several filtering methods, including textural and multilooking approaches, are generally used to reduce the speckle effect. However, such techniques usually also reduce the spatial resolution of the filtered SAR images. A common filtering solution that allows the speckle to be filtered without decreasing the SAR image spatial resolution is temporal averaging [24]. Certain land cover classes are characterized by radar signatures that are rather stable in time, such as the water class generally represented by very low backscattering values. Averaging SAR time series with a sufficient number of images permits a reduction in the speckle of the water class, making it separable from the land class. The Sentinel-1 mission is particularly well suited for applying this type of filtering since it allows us to regularly create dense SAR image stacks covering a relatively short period. Starting from the Sentinel-1 image intensity stacks, we first propose performing a pixelwise averaging operation in order to reduce the speckle effect. Then, the multitemporal intensity average will be used as a basis for extracting the coastline at the SAR data native resolution.

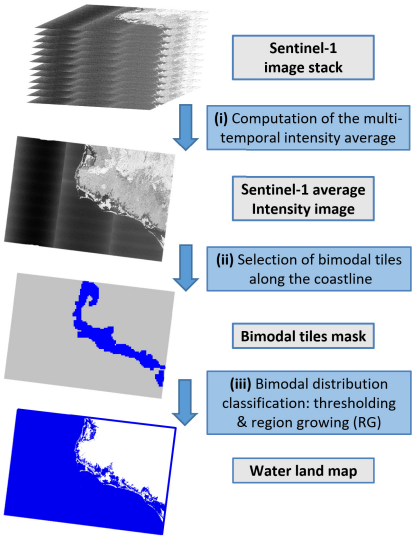

Fig. 1. Flowchart of the proposed algorithm.

For multitemporal filtered SAR images, we assume that the sea, as a smooth surface, exhibits low values, while land classes present higher values. From a statistical point of view, this specific characteristic can be represented by a bimodal distribution. Since coastal areas often represent just a fraction of SAR scenes, the parameterization of a bimodal distribution from an entire SAR image might be difficult, if not infeasible. Therefore, before applying any statistical processing, the SAR image must be divided into several tiles that are representative of the sea and land classes [23]. First, an iterative quadtree decomposition of the image into four equally sized tiles is performed. The bimodal tiles are identified via an adaptive thresholding operation. A tile is selected for threshold determination under the following conditions: the histogram is bimodal, the sea-land populations are normally, distributed, and each population represents at least 10% of the total population. The lowest tile decomposition level is fixed based on the minimum number of pixels guaranteeing statistical representativeness.

Based on the HSBA-selected tiles, we are able to estimate accurate sea-land PDFs for the entire SAR image. The Sentinel-1 Interferometric Wide (IW) swath mode variation effect of backscattering values depending on the incidence angle (29°–46°) is taken into account by the adaptive thresholding via HSBA. The extracted sea PDF is then employed to

generate the seed data of a region growing procedure. Within this step, the seeds are iteratively grown until a given tolerance level is reached. In order to find the optimal tolerance level, we minimize the root-mean-square error (RMSE) between the empirical distribution estimated from the region growing pixels and the theoretical sea PDF. This procedure allows the sea and land classes to be separated precisely.

III. Experimental Results

The SAR data set is composed of Sentinel-1 ground range detected (GRD) images in the IW swath mode, with a spatial resolution rg $\times$ az of approximately 5 $\times$ 20 m and dual-polarization channels (VV and VH). The coastline extraction is performed independently for both the VV and VH polarization channels. For each case study, a stack of ten Sentinel-1 images from the same orbital track, acquired over one year, is selected. The experiments were carried out using a computer with an i7-6800K CPU processor with 3.40 GHz and a memory of 64 GB. The proposed algorithm took about 10 min to extract the coastline from the multitemporal averaged intensity, i.e., an image of 14 300 $\times$ 10 800 pixels.

The results are evaluated through a comparison with open street map (OSM) coastline available globally (www.openstreetmap.org) as one of the largest sources of geographic information based on volunteer data collection and human mapping [25]. The OSM coastline is defined as the mean high water spring (i.e., point of the highest tide) line between the sea and the land. Sentinel-2 images are used for a qualitative evaluation of the results.

A. Quantitative SAR-OSM Cross Comparison

First, in order to analyze the overall performance of the SAR coastline detection method, we carry out a quantitative cross-comparison with the OSM coastline over two large areas of interest (AOIs). The AOIs, as shown in Fig. 2, comprise the entire coastline area of the Sinaloa state in Mexico (Gulf of California) and the coastline located in the south of Houston, USA, with total lengths of more than 500 and 200 km, respectively. In order to compute the coastline for the two AOIs, we have processed seven different Sentinel-1 IW image stacks. The comparison is realized in a buffer area with a width of 4 km selected across the OSM coastline in order to have the two classes, sea and land, well balanced. The overall agreement (OA) values, between the Sentinel-1 VV based coastline and the OSM one, defined as the total number of pixels classified as sea by both OSM and the proposed algorithm divided by the total number of pixels, are approximately 80.6% for the Sinaloa AOI and 90.4% for the South Houston AOI. The Sinaloa AOI is a complex coastal environment, including numerous mangrove areas and rocky shores. This aspect is likely to explain the lower OA with respect to the South Houston AOI, which is rather a coastal environment with various sand and bay areas. For the VH channel, the OAs are slightly lower than for the VV channel, approximately 77.3% for the Sinaloa AOI and 90.0% for the South Houston AOI. From the zoom-ins 1 and 2 shown at the top of Fig. 2, we notice that the OSM and Sentinel-1 coastlines show important differences for irregular shores composed of many inlets and bays, whereas, for regular/relatively straight shores, the two coastlines are very similar as shown in zoom-ins 3 and 4.

B. In-Depth Qualitative Analysis

The first case study focuses on an area extracted from the Sinaloa coastline, Mexico, containing vegetated areas that

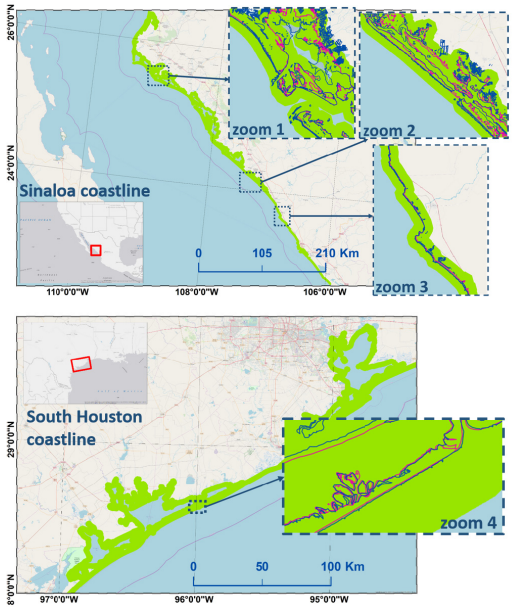

Fig. 2. Comparison between OSM (pink line) and VV SAR (blue line) coastlines within the AOI depicted in green: a buffer zone of 4-km width traced along the coastlines of (Top map) Sinaloa state, Mexico, and (Bottom map) South of Houston, USA.

are clearly visible in both the Sentinel-1 average intensity image and the Sentinel-2 image, as shown in Fig. 3(a)–(c). These vegetated areas correspond to mangrove forests [26] mainly located in the vicinity of aquacultural zones, e.g., shrimp farms. We can notice from Fig. 3(a) that a majority of mangrove areas are not mapped by the OSM coastline, whereas, in the Sentinel-1 average intensity image, this land class is represented by high backscattering pixel values that are accurately delineated in the SAR water–land map, as shown in Fig. 3(b). Moreover, we notice that despite the different polarimetric sensitivity of Sentinel-1 backscatter for VV and VH with respect to vegetation dynamics, the mangrove areas are delineated by the SAR coastline for both polarizations. In addition, we notice that the VV SAR-derived coastline allows us to delineate water–land classification details more accurately for both sand and aquacultural areas, as shown in Fig. 3(b). Fig. 3(c) shows a visual comparison between the SAR-detected coastline and a Sentinel-2 image from the area, thereby illustrating the capability of the SAR images to accurately delineate the shoreline for different types of coastal structures ranging from mangrove forests and large beaches to small cliffs and rocks. The zoom-in on the bottom left-hand side of Fig. 3(c) illustrates the added value of the SAR coastline with respect to the OSM for the mangrove areas.

The second case study focuses on shoreline detection in an area with classic coastal dynamic variations, such as tides, waves, or currents, located south of Houston in the Gulf of Mexico. A visual comparison between the OSM and SAR-based coastlines showcased in Fig. 3(d) and (e) indicates that for the regular/straight coastal areas covered by sand, the two coastlines are indeed very similar. In addition, the SAR-based coastline allows inland water bodies located in the vicinity of the coastline to be precisely detected. Fig. 3(f) shows a visual comparison between the SAR-detected coastline and a Sentinel-2 image from the area, demonstrating the capability of the SAR time series data to accurately detect the coastline and also smaller water bodies connected to sea waters, including rivers, lakes, and water channels. The zoom-in in the bottom

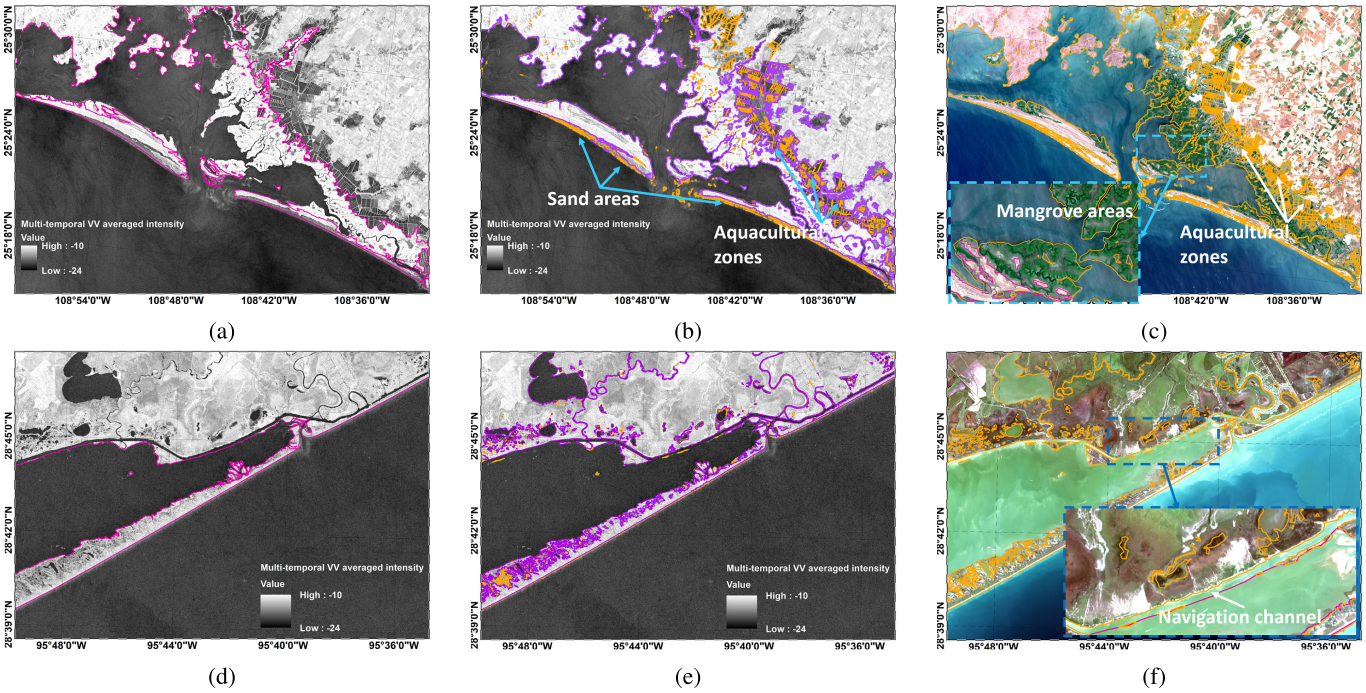

Fig. 3. Case studies. First row: Mexican coastline, Gulf of California. Second row: South of Houston, Gulf of Mexico. Sentinel-1 VV averaged intensity over 2019 and 2017 overlaid by (a) and (d) OSM (pink) and (b) and (e) SAR-derived VV (orange) and VH (violet) coastlines. (c) and (f) Sentinel-2 RGB image at 10-m resolution and overlaid SAR-derived VV (orange) coastline.

right-hand side of the figure illustrates that the SAR data allows the channel located in the north of East Matagorda Bay, which is completely masked in the OSM data, to be delineated precisely. For instance, having precise information about the channel location is important for monitoring ships that are navigating inside or in the proximity of the channel, as shown in Fig. 3(f).

C. Support for EO-Monitoring Applications in Coastal Areas

Several challenges arise when SAR-based ship- and flood-monitoring operational services are applied in coastal areas. In the following, we demonstrate that an accurate SAR coastline delineation can help in tackling such challenges.

Ship Detection Near the Coastline: An essential step in SAR-based ship detection is land masking, usually realized with a dedicated coastline, i.e., OSM or other coastline vector files. A buffer area is usually employed in order to account for any inaccuracies between the two data sources, but this leads to an underdetection of vessels located near the shoreline. Fig. 4 shows an example of an SAR image containing a vessel making its way in a navigation channel, as shown in the zoom-in area of the same figure. One can see that due to the new SAR-based coastline, no buffer needs to be applied for detecting vessels in such scenarios, while the OSM coastline masks the navigation channel, hindering the detection of such vessels.

Flood Mapping in Coastal Areas: Across the globe, many countries located in coastal areas are at high risk of damage caused by natural disasters. Numerous devastating water-related disasters have recently hit coastal regions all over the world. For example, in 2017, Hurricane Harvey hit Texas in August and September 2017, causing major flood damage in large areas surrounding Houston. The AOI addressed in Fig. 3(d)–(f) is located in the south of Houston and was affected by Harvey-related flooding. In order to precisely

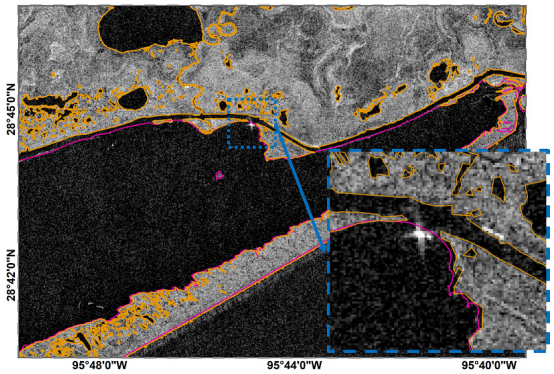

Fig. 4. Example of a ship located in a navigation channel in the coastline proximity of South Houston, USA: Sentinel-1 image (July 24, 2017), OSM coastline (pink), and SAR-VV coastline derived from the SAR averaged image over 2017 (orange).

delineate such a large size flood located in the proximity of the shoreline, it is essential to have access to information about the coastline, allowing us to more easily separate the floodwater from the permanent water bodies. Fig. 5(a) shows a subset of a Sentinel-1 image presenting a high sea state and acquired during the flood and the overlaid SAR coastline derived from the intensity average image over 2017. We can observe that the precise SAR-derived coastline makes it possible to identify the floodwater separately from the permanent water, i.e., flood extent. Fig. 5(b), illustrating a Sentinel-2 image acquired one day later, confirms the same large flood extent.

IV. Conclusion

In this letter, we propose an unsupervised and automatic method enabling precise detection of the coastline extent that encapsulates all its temporal variations by making use of the SAR time series. The tiling-based classification approach

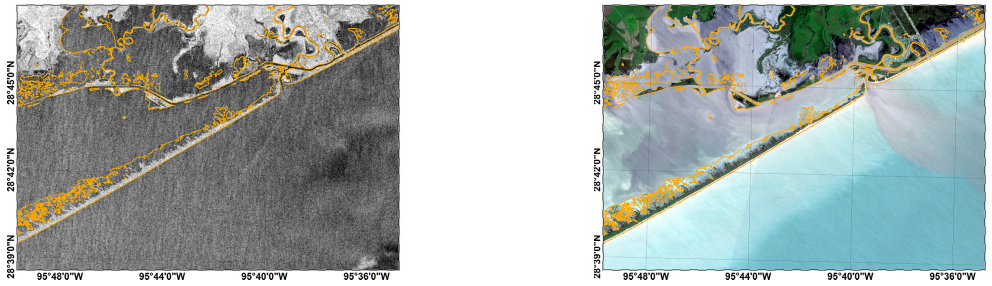

(a) (b)

Fig. 5. Flood caused by hurricane Harvey that hit the Texas coast (zoomed-in view on south of Houston): (a) Sentinel-1 image, August 29, 2017. (b) Sentinel-2, August 30, 2017. SAR-VV coastline derived from the SAR averaged image over 2017 (orange).

used allows us to separate the land and water classes in a computationally efficient manner. A large-scale comparison with an independent data set, i.e., OSM, shows a high agreement ranging from 80% to 90%, which is confirmed by several qualitative evaluations, including Sentinel-2 image samples. An in-depth analysis shows that the proposed method allows for the provision of more detailed coastline products that accurately detect vegetated areas as mangroves for the Sinaloa AOI or navigation channels for the South Houston AOI. The effectiveness of the SAR-based coastline illustrates that it is possible to improve the detection of vessels located in the shoreline proximity and to accurately map floods occurring in coastal areas. In order to surpass the limitations of the Sentinel-1 coastline product, e.g., for certain sand areas represented by low SAR backscattering values, in a future study, the Sentinel-2 time series could be integrated for further developing the proposed method.

ACKNOWLEDGMENT

The authors would like to thank G. Eiden and M. Nuevo from LuxSpace, Luxembourg for the useful discussions and the anonymous reviewers for their useful comments and suggestions that greatly improved this letter.

REFERENCES

[1] UN Atlas of the Oceans. *Human Settlements on the Coast*. Accessed: Oct. 28, 2019. [Online]. Available: http://www.oceansatlas.org/subtopic/en/c/114/

[2] J. R. Clark, "Multiple uses of the coastal zone," in *Integrated Management of Coastal Zones*. Rome, Italy: Food and Agriculture Organization of the United Nations, 1994.

[3] R. Gens, "Remote sensing of coastlines: Detection, extraction and monitoring," *Int. J. Remote Sens.*, vol. 31, no. 7, pp. 1819–1836, Apr. 2010.

[4] R. Pelich *et al.*, "Large-scale automatic vessel monitoring based on dual-polarization Sentinel-1 and AIS data," *Remote Sens.*, vol. 11, no. 9, p. 1078, May 2019.

[5] E. Politi, S. K. Paterson, R. Scarrott, E. Tuohy, C. O'Mahony, and W. C. A. Cámaro-García, "Earth observation applications for coastal sustainability: Potential and challenges for implementation," *Anthropocene Coasts*, vol. 2, no. 1, pp. 306–329, Jan. 2019.

[6] J.-S. Lee and I. Jurkevich, "Coastline detection and tracing in SAR images," *IEEE Trans. Geosci. Remote Sens.*, vol. 28, no. 4, pp. 662–668, Jul. 1990, doi: 10.1109/TGRS.1990.572976.

[7] D. C. Mason and I. J. Davenport, "Accurate and efficient determination of the shoreline in ERS-1 SAR images," *IEEE Trans. Geosci. Remote Sens.*, vol. 34, no. 5, pp. 1243–1253, Sep. 1996.

[8] M. Tello Alonso, C. Lopez-Martinez, J. J. Mallorqui, and P. Salembier, "Edge enhancement algorithm based on the wavelet transform for automatic edge detection in SAR images," *IEEE Trans. Geosci. Remote Sens.*, vol. 49, no. 1, pp. 222–235, Jan. 2011.

[9] M. Silveira and S. Heleno, "Separation between water and land in SAR images using region-based level sets," *IEEE Geosci. Remote Sens. Lett.*, vol. 6, no. 3, pp. 471–475, Jul. 2009.

[10] F. Baselice and G. Ferraioli, "Unsupervised coastal line extraction from SAR images," *IEEE Geosci. Remote Sens. Lett.*, vol. 10, no. 6, pp. 1350–1354, Nov. 2013.

[11] A. Buono, F. Nunziata, L. Mascolo, and M. Migliaccio, "A multipolarization analysis of coastline extraction using X-Band COSMO-SkyMed SAR data," *IEEE J. Sel. Topics Appl. Earth Observ. Remote Sens.*, vol. 7, no. 7, pp. 2811–2820, Jul. 2014.

[12] F. Nunziata, M. Migliaccio, X. Li, and X. Ding, "Coastline extraction using dual-polarimetric COSMO-SkyMed PingPong mode SAR data," *IEEE Geosci. Remote Sens. Lett.*, vol. 11, no. 1, pp. 104–108, Jan. 2014.

[13] X. Ding, F. Nunziata, X. Li, and M. Migliaccio, "Performance analysis and validation of waterline extraction approaches using single- and dual-polarimetric SAR data," *IEEE J. Sel. Topics Appl. Earth Observ. Remote Sens.*, vol. 8, no. 3, pp. 1019–1027, Mar. 2015.

[14] C. Liu, Y. Xiao, and J. Yang, "A coastline detection method in polarimetric SAR images mixing the region-based and edge-based active contour models," *IEEE Trans. Geosci. Remote Sens.*, vol. 55, no. 7, pp. 3735–3747, Jul. 2017.

[15] M. Modava, G. Akbarizadeh, and M. Soroosh, "Integration of spectral histogram and level set for coastline detection in SAR images," *IEEE Trans. Aerosp. Electron. Syst.*, vol. 55, no. 2, pp. 810–819, Apr. 2019.

[16] N. Demir, M. Kaynarca, and S. Oy, "Extraction of coastlines with fuzzy approach using Sentinel-1 SAR image," *Int. Arch. Photogramm., Remote Sens. Spatial Inf. Sci.*, vol. 41-B7, pp. 747–751, Jun. 2016.

[17] Z. Liu, F. Li, N. Li, R. Wang, and H. Zhang, "A novel region-merging approach for coastline extraction from sentinel-1A IW mode SAR imagery," *IEEE Geosci. Remote Sens. Lett.*, vol. 13, no. 3, pp. 324–328, Mar. 2016.

[18] F. Nunziata, A. Buono, M. Migliaccio, and G. Benassai, "Dual-polarimetric C- and X-band SAR data for coastline extraction," *IEEE J. Sel. Topics Appl. Earth Observ. Remote Sens.*, vol. 9, no. 11, pp. 4921–4928, Nov. 2016.

[19] D. Ao, O. Dumitru, G. Schwarz, and M. Datcu, "Coastline detection with time series of SAR images," *Proc. SPIE*, vol. 10422, Oct. 2017, Art. no. 104220U.

[20] F. Bioresita and N. Hayati, "Coastline changes detection using Sentinel-1 satellite imagery in Surabaya, East Java, Indonesia," *J. Geodesy Geomatics*, vol. 11, pp. 190–198, Feb. 2016.

[21] D. Di Luccio *et al.*, "Shoreline rotation analysis of embayed beaches by means of *in situ* and remote surveys," *Sustainability*, vol. 11, no. 3, p. 725, Jan. 2019.

[22] H. Liu, L. Wang, D. J. Sherman, Q. Wu, and H. Su, "Algorithmic foundation and software tools for extracting shoreline features from remote sensing imagery and LiDAR data," *J. Geographic Inf. Syst.*, vol. 3, no. 2, pp. 99–119, 2011.

[23] M. Chini, R. Hostache, L. Giustarini, and P. Matgen, "A hierarchical split-based approach for parametric thresholding of SAR images: Flood inundation as a test case," *IEEE Trans. Geosci. Remote Sens.*, vol. 55, no. 12, pp. 6975–6988, Dec. 2017.

[24] M. Chini, R. Pelich, R. Hostache, P. Matgen, and C. Lopez-Martinez, "Towards a 20 m global building map from Sentinel-1 SAR data," *Remote Sens.*, vol. 10, no. 11, p. 1833, Nov. 2018.

[25] M. F. Goodchild, "Citizens as sensors: The world of volunteered geography," *GeoJournal*, vol. 69, no. 4, pp. 211–221, Nov. 2007.

[26] R. Hernández Cornejo, N. Koedam, A. Ruiz Luna, M. Troell, and F. Dahdouh-Guebas, "Remote sensing and ethnobotanical assessment of the mangrove forest changes in the Navachiste-San Ignacio-Macapule Lagoon complex, Sinaloa, Mexico," *Ecology Soc.*, vol. 10, no. 1, pp. 1–19, 2005.